JOURNAL OF GEOPHYSICAL RESEARCH, VOL. 99, NO. D2, PAGES 3517-3532, FEBRUARY 20, 1994

The reaction probability of N_2O_5 with sulfuric acid aerosols at stratospheric temperatures and compositions

Alan Fried, Bruce E. Henry, and Jack G. Calvert
National Center for Atmospheric Research, Boulder, Colorado

Michael Mozurkewich
Department of Chemistry and Centre for Atmospheric Chemistry, York University, North York, Ontario, Canada

We have measured the rate of reaction of N_2O_5 with H_2O on monodisperse, submicrometer H_2SO_4 particles in a low-temperature flow reactor. Measurements were carried out at temperatures between 225 K and 293 K on aerosol particles with sizes and compositions comparable to those found in the stratosphere. At 273 K, the reaction probability was found to be 0.103 ± 0.006, independent of H_2SO_4 composition from 64 to 81 wt %. At 230 K, the reaction probability increased from 0.077 for compositions near 60% H_2SO_4 to 0.146 for compositions near 70% H_2SO_4. Intermediate conditions gave intermediate results except for low reaction probabilities of about 0.045 at 260 K on aerosols with about 78% H_2SO_4. The reaction probability did not depend on particle size. These results imply that the reaction occurs essentially at the surface of the particle. A simple model for this type of reaction that reproduces the general trends observed is presented. The presence of formaldehyde did not affect the reaction rate.

Introduction

It is now well established that a substantial depletion of stratospheric ozone occurs during the Antarctic spring [*Solomon*, 1988]. The high rates of ozone destruction are caused by high concentrations of active chlorine (Cl and ClO) released from inactive forms by means of heterogeneous reactions occurring on the surfaces of polar stratospheric cloud particles [*Kawa et al.*, 1992; *Turco et al.*, 1989]. Similar reactions occurring on the background stratospheric sulfate aerosol may have a significant effect on the chemistry of the global stratosphere. The possible consequences of these reactions during periods of enhanced aerosol loading following volcanic eruptions is of particular concern [*Brasseur et al.*, 1990; *Granier and Brasseur*, 1992; *Prather*, 1992]. After the eruption of El Chichón in 1982, significant amounts of nitrogen oxides were lost [*Roscoe et al.*, 1986]. Ozone depletion was also observed at midlatitudes [*Hofmann and Solomon*, 1989]. *Johnston et al.* [1992] have observed depletion of stratospheric NO_2, and *Grant et al.* [1992] have observed depletion of stratospheric ozone following the eruption of Mount Pinatubo. The extent to which heterogeneous reactions are responsible for these effects is not yet known. Since Mount Pinatubo injected more SO_2 into the stratosphere than El Chichón, the resulting perturbations are expected to be more intense and longer lasting [*Granier and Brasseur*, 1992].

One of the important heterogeneous reactions involving H_2SO_4 particles in the stratosphere is

$$N_2O_5 + H_2O \text{ (sulfate aerosol)} \rightarrow 2HNO_3 \quad (1)$$

In the stratosphere, N_2O_5 is in equilibrium with NO_2 and NO_3:

$$N_2O_5 \rightleftharpoons NO_2 + NO_3. \quad (2)$$

Paper number 93JD01907.
0148-0227/94/93JD-01907$05.00

Reaction (1) will reduce stratospheric NO_2 concentrations and increase the concentrations of ClO and OH radicals by reducing the rates of the reactions

$$ClO + NO_2 + M \rightarrow ClONO_2 + M \quad (3)$$

$$OH + NO_2 + M \rightarrow HNO_3 + M. \quad (4)$$

Increased OH leads in turn to increased active chlorine by means of

$$OH + HCl \rightarrow H_2O + Cl. \quad (5)$$

The increase in active chlorine due to suppression of (3) and enhancement of (5) results in a reduction in ozone concentrations [*Pitari et al.*, 1991; *Rodriguez et al.*, 1991]. Modeling studies indicate that this reaction sequence alone is not the complete picture, since including (1) improves agreement with measured distributions of stratospheric HNO_3 but reduces agreement between calculated and measured NO_x ($NO + NO_2$) [*Austin et al.*, 1986; *Considine et al.*, 1992; *Granier and Brasseur*, 1992].

The rates of heterogeneous reactions are usually expressed in terms of the fraction of collisions between a molecule and a surface which results in reaction. This fraction is called the reaction probability, γ, and is sometimes also referred to as the sticking coefficient. Previously reported values of γ for reaction (1) are given in Table 1. The values of γ measured on H_2SO_4/H_2O surfaces with compositions of less than 80% H_2SO_4 are within a factor of 3 of each other. These results imply a stratospheric lifetime for N_2O_5 of a few days on background aerosols at 20 km, short enough to have a significant impact on stratospheric chemistry. However, each of these experiments determined γ for only a few temperatures and liquid-phase compositions.

Only the results of *Mozurkewich and Calvert* [1988], over a limited range of temperatures and H_2SO_4 compositions were obtained with particles of sizes comparable to those found in the atmosphere. There are two reasons why the particle size might affect γ. First, the Kelvin effect will cause both gas

TABLE 1. Reported Values of the Reaction Probability γ for N_2O_5 on H_2SO_4 Surfaces

Composition (H_2SO_4, wt %)	Diameter μm	Temperature, K	Reaction Probability	Reference
83-100	bulk	214-263	10^{-4} - 10^{-5}	(1)
>95	bulk	300	>3.8x10^{-5}	(2)
65-75	0.08 - 0.2	274	0.14	(3)
65-75	0.08 - 0.2	293	0.10	(3)
73	200	283	0.06	(4)
40-75	bulk	215-230	0.10-0.14	(5)
73-95	bulk	223	>0.06	(6)

References: 1, *Harker and Strauss* [1981]; 2, *Baldwin and Golden* [1979]; 3, *Mozurkewich and Calvert* [1988]; 4, *Van Doren et al.* [1991]; 5, *Hanson and Ravishankara* [1991]; 6, *Golden et al.* [1993].

solubilities and particle compositions to vary with particle size. Although in theory we expect this effect to be small, it is desirable to verify this experimentally. Second, the relative importance of mass transport and chemical reaction contributions to the overall rate will depend on particle size [*Schwartz and Freiberg*, 1981; *Schwartz*, 1986]. As shown in the data analysis section, there should be a particle size below which γ decreases with decreasing size. Measurements using small particles provide results that are complementary to those obtained using bulk surfaces and provide greater confidence in extrapolating laboratory results to the stratosphere. As shown in Table 1, most laboratory results for (1) fall in the range 0.06 to 0.14. Stratospheric models, however, require γ to be better defined. For background aerosol conditions, a factor of 2.5 change in γ produces a change up to a factor of 2 in the calculated NO_x/NO_y ratio at midlatitudes (S. R. Kawa, personal communication, 1992).

In this paper we present laboratory measurements of γ for (1) for liquid-phase H_2SO_4 compositions from 54 to 82 wt % (hereafter, all aerosol compositions are given in weight percent) and temperatures of 225 to 293 K. These measurements were made on monodisperse aerosol particles; the particle diameter was varied from 0.060 to 0.250 μm. The measurement technique is similar to that used by *Mozurkewich and Calvert* [1988]; however, a number of refinements have been made to improve the accuracy and to extend the range of conditions that may be investigated.

Experimental Method

Aerosol Generation

Aerosol generation experiments were conducted by combining N_2O_5 and H_2SO_4 aerosol flows in a flow tube reactor and observing the decay of the N_2O_5 concentration with time. A flow diagram of the aerosol source is shown in Figure 1. The aerosol source produced H_2SO_4 particles by homogeneous nucleation resulting from the reaction of SO_3 with H_2O. This was chosen because atomizers, as used previously by *Mozurkewich and Calvert* [1988], produce droplets with diameters mostly in excess of 1 μm. It is difficult to use electrostatic methods to classify such large particles because of

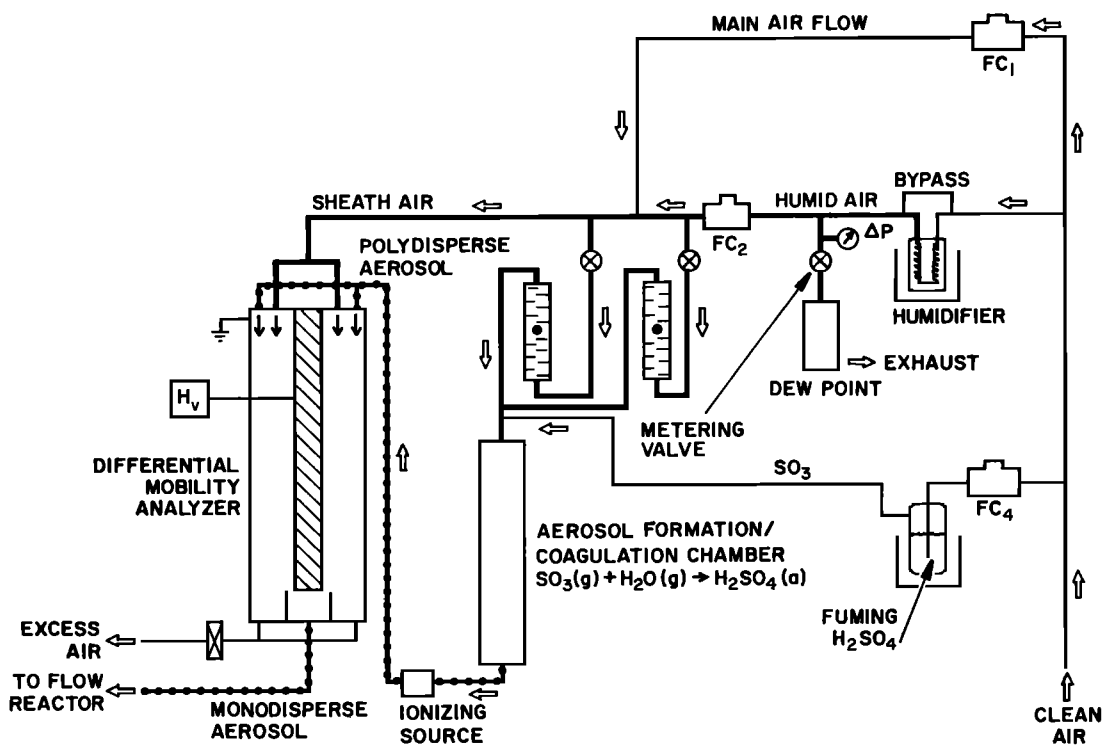

Fig. 1. Flow diagram of the aerosol source; FC in this and Fig. 2 are flow controllers.

multiple charging. Smaller particles could be produced by atomizing dilute aqueous solutions and evaporating the excess water; however, it is very difficult to dry the resulting aerosol to the levels needed for these experiments.

Zero air was provided by an Aadco clean-air supply and was split into three streams. One stream, approximately 1500 sccm, (cm^3 min^{-1} at STP) was humidified in order to control the amount of water vapor present in the experiment. The humidifier consisted of a 1-m length of GoreTex tubing immersed in either deionized or distilled water in a temperature-controlled bath. The flow to be humidified was split into two parts by means of flow restrictors. If relatively large H_2O concentrations were desired, the two parts were combined before they passed through the humidifier. For lower concentrations the flows were combined downstream of the humidifier so that only the smaller flow (1/30th of the total) was humidified. Up to 1000 sccm of this humid airflow, regulated by a mass flow controller, was used for the experiments; the remainder was passed though a dew point hygrometer (EG&G model 911) to determine the water vapor partial pressure. Measured partial pressures typically agreed to within 2% with those expected from the humidifier temperature and pressure.

The second clean-air stream (about 9000 sccm) constituted the main airflow; this was mixed with the humid air, and the combined flow was split into two parts. The larger part was used for the differential mobility analyzer (DMA) sheath flow, and the smaller part (500 to 1500 sccm) was sent to the aerosol source. At H_2O concentrations of less than about 200 ppm by volume (ppmv), the source produced few particles. Therefore for experiments at low H_2O concentrations, a portion of the humid airflow (measured by a rotameter) was sent directly to the aerosol source rather than being mixed with the main air flow. With this humidification technique, we were able to obtain H_2O mixing ratios of 8 to 1700 ppmv in the flow reactor. The relative humidities used in the experiments ranged from 0.2 to 22% at 273 K (H_2O concentrations of 26 to 1700 ppmv) and 2 to 20% at 230 K (H_2O concentrations of 8 to 46 ppmv). The resulting particle compositions are 55 to 81% H_2SO_4 at 273 K and 53 to 71% at 230 K.

The third clean-air stream (up to 100 sccm) was bubbled through fuming sulfuric acid (18-24% SO_3 by weight) in order to provide SO_3 to the aerosol source. The outlet of the bubbler was fitted with a glass frit to trap any particles produced by bubble bursting. Mixing the SO_3 flow with a portion of the humidified main airflow resulted in the nucleation of a large number of particles. These were allowed to grow by coagulation during passage through a 94-cm length of 1.7-cm-ID stainless steel tubing. The mean diameter of the resulting particles could be varied by changing both the amount of SO_3 (and therefore the total particle mass) and the total flow through the source to vary the time allowed for coagulation. Measured size distributions of the aerosol produced in this source typically had logarithmic standard deviations of 0.35 to 0.4; this is close to the values expected for self-preserving distributions [*Lee et al.*, 1984]. These narrow size distributions minimize double charging and maximize the number densities of monodisperse aerosol that can be selected by electrical mobility classification. The occurrence of self-preserving size distributions indicates that the nucleation process is rapid compared to the residence time in the coagulation chamber. This in turn implies that the SO_3 is probably completely consumed in the aerosol source, a conclusion that is supported by kinetic modeling of the nucleation process (L. Phillips, private communication, 1993).

The aerosol flow from the coagulation chamber was passed over a 500-μC; ^{210}Po source to establish a Boltzmann charge distribution [*Liu and Pui*, 1974]. The charged particles were admitted to the DMA, where they migrated into the sheath airflow under the influence of an electric field [*Knutson and Whitby*, 1975]. A small fraction of the sheath flow (typically 1500 sccm) was withdrawn at the exit of the DMA; all particles in this flow have very nearly the same electrical mobility. Particles of a desired mobility are selected by adjusting the voltage applied in the DMA. The electrical mobility is a function of both particle size and charge; for particles of a given charge, the size distribution exiting the DMA is sharply peaked, with a half width of about 5% of the mean. The absolute size of particles produced by this method is accurate to within a few percent. By setting the DMA voltage to zero, particle-free air could be supplied to the flow reactor without changing the composition of the air or disturbing any of the flows, a procedure which was necessary in determining the rate of reaction on the flow reactor walls. For some experiments the aerosol charge at the DMA output was neutralized using a ^{85}Kr source. However, charged aerosol particles without this neutralization gave identical results.

The particle size selected by the DMA was used together with measurements of number density to compute a surface area. Most of the particles were singly charged; however, a small fraction were doubly charged. These were larger than the singly charged particles and therefore had greater surface areas. To determine the number of doubly charged particles, the DMA voltage was adjusted so as to pass the singly charged particles of this larger size. The number density of the doubly charged particles was calculated by assuming that they were in Boltzmann equilibrium with the singly charged particles. The extra surface area due to these larger particles was calculated and included in the calculated aerosol surface area. These corrections were typically 10 to 20%.

The monodisperse aerosol flow from the DMA (1000 to 3000 sccm) constituted the main part of the flow admitted to the flow reactor. Although the DMA was operated at ambient pressure and temperature, the flow reactor was often operated at reduced pressure to lower the partial pressures of H_2O and N_2O_5. The pressure of the monodisperse aerosol flow was reduced to that of the flow reactor by means of a pair of stainless steel straight-through valves. Normal flow-regulating valves removed 90% of 0.105-μm-diameter particles in reducing the pressure from 800 to 530 mbar. With the straight-through valves, losses were minor at a flow reactor pressure of 470 mbar and amounted to 34% at 330 mbar. We found that the Delrin seats in these valves produced formaldehyde, apparently by reacting with H_2SO_4. Accordingly, the Delrin seats were replaced with stainless steel seats, although the formaldehyde proved to have no effect on the results. In a large number of experiments, the pressure drop was achieved using a 0.51-mm- diameter stainless steel orifice in place of the straight-through valves to achieve better stability of the flow reactor pressure.

Laminar-Flow Reactor

A diagram of the flow reactor is shown in Figure 2. Before entering the flow reactor, the aerosol was passed through an external glass heat exchanger (not shown) to minimize

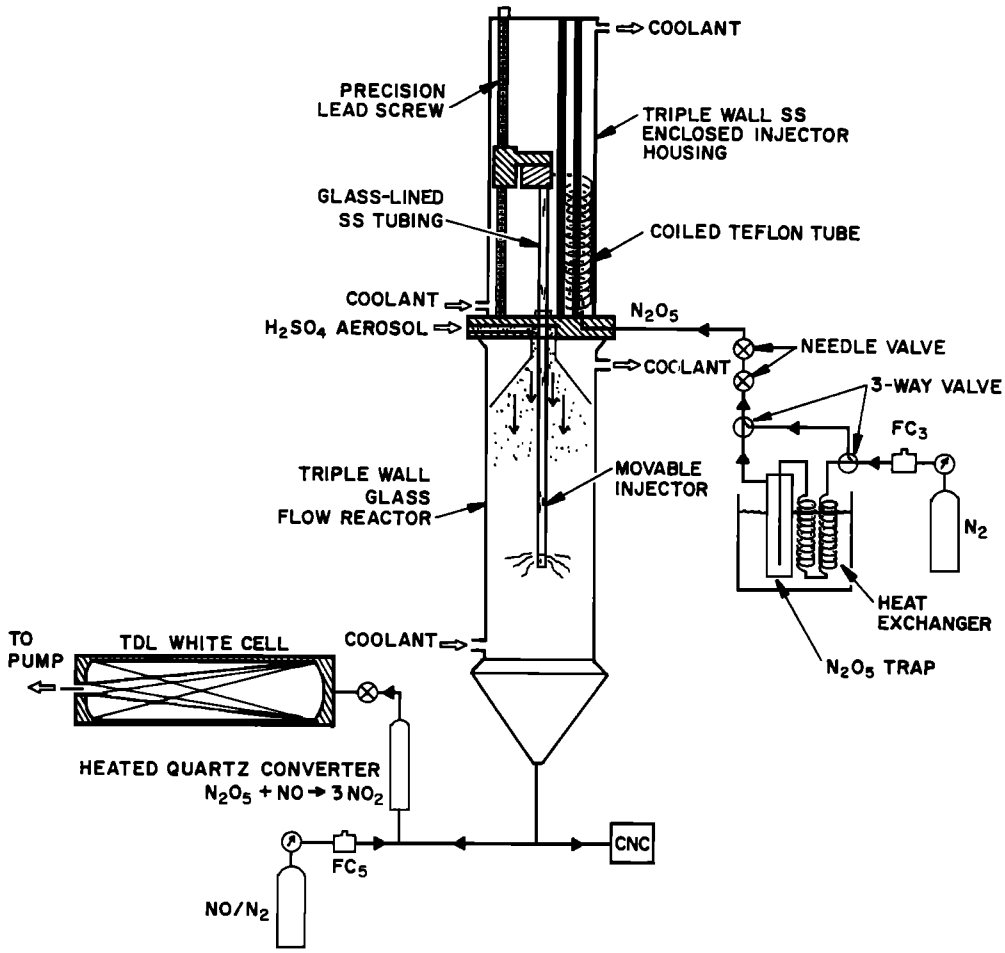

Fig. 2. Flow diagram of the apparatus for measuring the N_2O_5 reaction probability with aerosol particles. SS, stainless steel.

temperature gradients in the flow reactor. The heat exchanger, flow reactor, inlet flange, and enclosed injector system (described in a following section) were all maintained at a uniform temperature by circulating ethanol from an external constant temperature bath (Neslab model ULT-80DD). Both the flow reactor and the injector system were equipped with outer vacuum jackets for insulation.

The Pyrex flow reactor had an inside diameter of 48.1 mm ± 0.5 mm and an overall length of 125 cm, 107 cm of which was temperature controlled. The reactor was mounted vertically with the flow passing downward through it. As shown in Figure 2, the aerosol was admitted into the flow reactor at a fixed position through a 13-cm-long glass diffuser cone which expands at a 7° half angle; this minimizes the production of turbulent eddies at the inlet. During the measurement of an N_2O_5 decay, the walls of the entire reaction zone were exposed to a constant aerosol loading. The aerosol was exposed only to components made of glass and stainless steel. Teflon was avoided, since it enhances the electrostatic deposition of charged particles [*McMurry and Rader*, 1985].

Calibrated thermocouples were used to measure the inlet gas temperature at the exit of the diffuser cone and the wall temperature at the exit of the flow reactor. Over the temperature range studied, 225 to 293 K, the temperature difference over the length of the flow reactor was typically 0.2 K. Temperature gradients must be kept small, since high-pressure flows in large diameter tubes are susceptible to thermal convection. The driving force for convection is quantified by the Rayleigh number *Ra*, defined by

$$Ra = \frac{gR^4\rho^2 C_p}{T\eta\kappa}\left[\frac{dT}{dZ}\right], \tag{6}$$

where g is the acceleration of gravity; R is the flow reactor radius; Z is the distance along the axis of the tube; and ρ,C_p, η, and κ are the density, specific heat, viscosity, and thermal conductivity of the gas respectively. In horizontal tubes some convection occurs for all nonzero values of *Ra*. In vertical tubes with a cooled downward flow and a Reynolds number greater than 80, the flow is disturbed by convection if *Ra* exceeds a critical value of 75 [*Yao*, 1987*a*, *b*]. At lower Reynolds numbers, the critical *Ra* should be larger, since it is infinite for a stationary column of air. The Reynolds numbers used in these experiments were typically about 50. Even in the worst case (low temperature, high pressure), a temperature difference of 0.2 K implies $Ra < 20$, which is well within the limit for stable laminar flow.

Aerosol Characterization

For the range of particle sizes used (0.060- to 0.25-μm diameter), diffusional and settling losses are minimal. However, in cooling the flow to low temperatures,

thermophoretic losses [*Walker et al.*, 1979] could be as much as 20%. Because of the possibility of losses in the inlet system, the aerosol number densities were measured at the flow reactor exit by drawing a small sample (typically 1 to 2 cm^3 s^{-1}) from the center of the exit flow. Since the flow warms as it leaves the reactor, thermophoresis could concentrate particles in the center of the flow. However, the warming of the flow should induce considerable thermal convection, which would prevent this concentration from occurring.

The number density was measured with a TSI model 3760 condensation nucleus counter (CNC). This instrument detects individual particles. At pressures over 200 mbar, the counting efficiency of this type of CNC for particles larger than 0.060-μm diameter is very near unity [*Zhang and Liu*, 1991]. The sample flow rate was determined by drawing the sample flow through a capillary tube (0.93-mm ID, 10 cm long) and measuring the resulting pressure drop. This flow was then diluted with filtered room air to provide the total flow (25 cm^3 s^{-1}) required by the CNC. The number density was determined from the frequency of particle counts and the sample flow rate. The CNC is limited to number densities below 4 x 10^4 cm^{-3}. By diluting the sample, number densities in the flow reactor of up to 1 x 10^6 cm^{-3} could be measured. Particle losses in the capillary were not significant. This was checked at low number densities by comparison with a second CNC that did not sample through a capillary.

There is some coagulation of particles during the passage of the aerosol through the flow reactor. Electrostatic scattering [*Fuchs*, 1964] can also be significant. For an aerosol with a net charge, mutual repulsion of the particles results in enhanced deposition on the walls. Both coagulation and scattering will result in the actual number density in the flow reactor being larger than that measured by the CNC at the outlet. For each run, estimates of the effect of both processes on the aerosol surface area were made and suitable corrections were applied. These corrections were each typically less than 1%.

The relative humidity in the flow reactor is different from that in the DMA because of both the change in temperature and the addition of the flow carrying the N_2O_5. As a result, the amount of water in the particles and therefore the sizes of the particles will change. To account for this, we used the equations of *Gmitro and Vermeulen* [1964] with measured temperatures and H_2O partial pressure to compute the change in particle composition. This was combined with the density data tabulated by *Perry and Chilton* [1978] to compute the change in particle size. As described earlier, to achieve low water vapor concentrations it was necessary to direct some of the humid air directly into the aerosol coagulation chamber. Under these conditions the aerosol source and DMA sheath airflows had different relative humidities, and there was some ambiguity in computing the particle composition exiting the DMA. However, this introduces little uncertainty in the surface area, since the particle size is not a strong function of relative humidity under the dry conditions for which this procedure was necessary.

To verify the calculated dependence of particle size on relative humidity, we used the tandem DMA method of *Rader and McMurry* [1986]. The experiment was carried out at room temperature. A monodisperse H_2SO_4 aerosol at a relative humidity of 0.5% was produced using the procedure described earlier. A portion of the filtered sheath air from the source DMA was humidified and mixed with the rest of the sheath airflow and the monodisperse aerosol flow to produce a humidified aerosol flow. Part of this flow was used as the aerosol input to a second DMA that was used to determine the sizes of the humidified particles. The remaining flow was filtered and used for the sheath airflow; this ensured that there was no change in particle composition in the second DMA. A comparison of the measured and calculated diameter ratios is shown in Figure 3. The final diameter was systematically about 1% smaller than expected; this was observed even if the air was not humidified at all and is consistent with normally observed

The overall performance of the aerosol system was tested by means of a tandem DMA experiment with the second DMA placed downstream of the flow reactor. A CNC was used as described earlier to measure the particle number density exiting the flow reactor. The rest of the reactor outflow (1120 sccm) was passed through the second DMA. The filtered sheath airflow from the first DMA was used as the sheath air for the second DMA. Particle size distributions measured with the second DMA were analyzed by the method of *Rader and McMurry* [1986]. The absolute particle size, number density, and distribution width agreed with expected values to within the normal experimental errors of the instruments. Varying the flow reactor temperature from 273 to 235 K had no effect on the results, since the aerosol warmed up to room temperature after leaving the flow reactor. The number densities of coagulated particles were consistent with calculated values but were too low to be determined accurately.

N_2O_5 Source and Injector System

Solid N_2O_5 was prepared in a Pyrex trap according to the method of Davidson [*Cantrell et al.*, 1987]. The system for eluting N_2O_5 from this trap and transferring it to the flow reactor is shown in Figure 2. Both the trap and a coiled heat exchanger were maintained at constant temperature (typically 195 K with a stability of ±0.2 K) using a second Neslab ULT-80DD bath. The N_2O_5 vapor pressure stability was approximately ±4%. A controlled flow (100 to 250 sccm) of ultrahigh-purity nitrogen was passed through the heat exchanger and the N_2O_5 trap. This flow could also be diverted around the trap for zeroing the N_2O_5 signal. The N_2O_5 saturated flow then passed through a pair of glass/Teflon needle valves

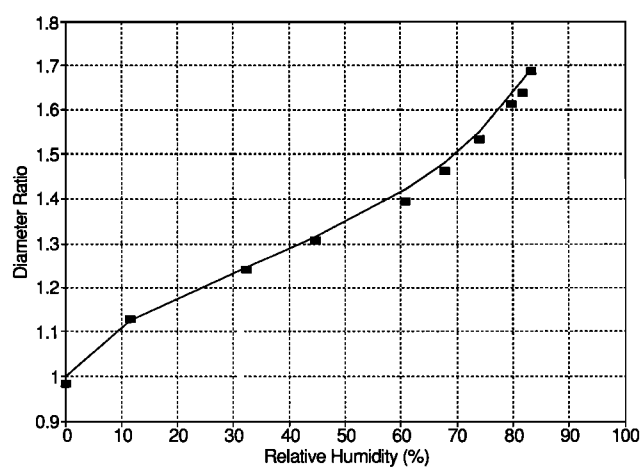

Fig. 3. Increase in particle size due to increase in relative humidity. The sizes are given as ratios of the diameters to a diameter of 144 nm for the particles produced at a relative humidity of 0.5%. The points are measured values, and the curve is calculated at each of the discrete measurement points as described in the text.

and through approximately 15 cm of opaque Teflon tubing (3 mm OD) before entering the enclosed injector system.

The needle valves were used to maintain the N_2O_5 trap at pressures slightly above ambient pressure rather than at the reduced pressures of the flow reactor. This precaution was taken to avoid potential leakage of ambient water vapor into the N_2O_5 trap. Care was taken to minimize exposure of the N_2O_5 vapor to metal surfaces; after exiting the trap, the N_2O_5 contacted only three stainless steel fittings. Approximately 40-60% of the initial N_2O_5 made it through this inlet system as compared to less than 10% when stainless steel tubing and fittings were used. Typical flow reactor N_2O_5 mixing ratios were between 30 and 200 ppbv at pressures between 333 and 800 mbar.

The N_2O_5 entered the flow reactor through an enclosed injector system that is described in detail elsewhere (B. Henry et al., Enclosed flow tube injector system for low temperature kinetic studies, to be submitted to *Rev. Sci. Instrum.*, 1994). Within the enclosure the N_2O_5 flow passed through a coiled section of 3-mm-OD Teflon tubing, a Delrin connector, and an injector tube consisting of a 120-cm length of precision OD (6.35 ± 0.05 mm OD) glass-lined stainless steel tubing. The enclosure was flushed with a slow flow of dry air and maintained at the same temperature and pressure as the flow reactor. The injector was connected to an external crank by means of a precision stainless steel lead screw, which was used to move the injector in and out of the flow tube through a sliding seal consisting of a Teflon-encapsulated Viton O-ring. A chevron seal external to the top of the injector chamber further prevented ambient moisture from reaching the internal seal and injector drive mechanism. This enclosed injector system offered a number of advantages. First, all surfaces that the N_2O_5 encountered were kept at a constant temperature so that the extent of decomposition of N_2O_5 did not change as the injector was moved in and out of the flow reactor. Second, temperature gradients that would otherwise arise from the movement of a warm injector into the cold flow reactor were minimized. Finally, enclosing the injector eliminated the introduction of impurities such as H_2O vapor into the flow reactor.

At the end of the injector tube, the N_2O_5 passed through a stainless steel fitting with six evenly spaced, 0.8-mm-diameter radial holes. The mixing of this flow (200 to 250 sccm) with the aerosol flow in the reactor was examined using NO in place of N_2O_5. The radial uniformity of the injected NO was determined by sampling approximately 7% of the flow through a sample tube, which was bent so that different radial positions could be sampled by rotating the tube. NO concentrations were measured as described in the following subsection. With zero separation between the injector and the sampler, the NO concentration at the walls was only 1% of that at the center line. At a separation of 15 cm, the average NO concentration was uniform to within 6%. This is consistent with the rate of diffusional mixing from a position halfway between the center line and the flow tube walls.

Measurement of N_2O_5 and H_2O Concentrations

NO was added to the flow exiting the flow reactor, and this was passed through a hot (130°C) quartz converter in which the N_2O_5 was thermally decomposed. As discussed by *Fahey et al.* [1985], one NO molecule is consumed and three NO_2 molecules are produced for every N_2O_5 molecule decomposed. This flow was then passed through a glass fiber filter (Gelman type A/E) and into an absorption cell of a tunable diode laser absorption spectroscopy (TDLAS) system for measurement of the NO concentration. Either NO or NO_2 can be measured by TDLAS with high sensitivity; however, the N_2O_5 spectral features are too dense for measurement by TDLAS.

Because of the potential for greater sensitivity, we initially employed measurements of the NO_2 produced. However, we found that the background NO_2 concentration changed as a function of the injector position. This appeared to be due to N_2O_5 decomposition in the inlet. This problem was especially severe when a conventional injector design (neither enclosed nor temperature controlled) was used. A greater injector length protruding out of the cold flow reactor resulted in the generation of higher background NO_2 concentrations. However, even with the enclosed injector, we found evidence that NO_2 was produced by N_2O_5 decomposition on the flow reactor walls. When N_2O_5 was measured as NO_2, it appeared to decay to a nonzero background concentration. This background changed from run to run, depending on the H_2O concentration, the initial N_2O_5 concentration, and the amount of aerosol surface area. This complication resulted in large and variable systematic errors and made it impossible to obtain reproducible results. Thus NO_2 product determination was abandoned.

Measurements of N_2O_5 made by determining the amount of NO consumed were not subject to these problems. With N_2O_5 present and no NO added to the converter, we carried out NO measurements at different injector positions. When large concentrations of H_2SO_4 particles were present, we measured an average NO concentration of 0.6 ppbv and a difference of 0.5 ± 0.5 ppbv with the injector at the top and bottom of the flow reactor. The corresponding values when no particles were added were 1.8 ppbv and 0.6 ± 0.5 ppbv, respectively. Since these amounts are smaller than the typical scatter (±4 to 6 ppbv) in N_2O_5 measurements, production of NO in the flow reactor should not cause significant systematic errors in our measurements in most circumstances. The one exception occurs after the walls have been exposed to high aerosol concentrations for an extended period of time, particularly when operating with high relative humidities and low flow reactor temperatures. This will be discussed further in the Results and Discussion section.

A number of tests were carried out to confirm the proper operation of the converter. As long as sufficient NO was added, (i.e., at least three times the N_2O_5 concentration) and the converter temperature was above approximately 130°C, the amount of NO consumed by N_2O_5 was independent of the amount of added NO and the converter temperature. Adding nitric acid, the product of the aerosol reaction, at concentrations up to 100 ppbv to the converter changed the NO concentration by less than 5%. If N_2O_5 was not present, the temperature of the converter had no effect on the added NO concentration.

As described earlier, a dew point hygrometer was used to determine the water vapor concentration added to the aerosol source. Because of the limited sensitivity of this instrument and the presence of some water vapor in the zero air, this did not provide an accurate determination of the flow reactor H_2O concentration when it was below about 200 ppmv. Since the H_2O concentration determined the aerosol composition, accurate measurements were made using TDLAS.

The tunable diode laser system has been described in detail by *Fried et al.* [1991], and only a brief description is given here. The diode laser employed in these measurements was

operated at temperatures near 100 K using a liquid-nitrogen dewar. The emerging IR radiation was passed through a 1.5-m bas path multipass White cell (Unisearch Inc.) and onto an InSb detector. The White cell was typically operated using a path length of 119 m and a pressure of 33 mbar (25 torr). Absorption signals were processed using second harmonic detection coupled with sweep integration. Typically, five scans, each averaged for 20 s, were acquired and averaged.

Water vapor was measured simultaneously with NO. Both features were recorded in the same diode laser scan, as described by *Fried et al.* [1993]. Each feature was independently fit to its own reference standard. Two different line pairs were employed at different times for these measurements. One used an H_2O line at 1820.3645 cm^{-1} and an NO doublet centered at 1820.414 cm^{-1}; the other used an H_2O line at 1816.0589 cm^{-1} and an NO doublet centered at 1816.5455 cm^{-1}. When the latter pair was used, the H_2O vapor feature was scanned and the diode laser current was then jumped to acquire the NO doublet. A typical 20-s averaged scan using the second line pair is shown in Figure 4.

The response of the TDLAS to NO was calibrated daily by diverting the N_2O_5 carrier flow past the N_2O_5 trap and obtaining an NO reference spectrum. The concentration of the NO/N_2 mixture was determined by comparison with National Institute of Standards and Technology standard reference mixtures. When measuring N_2O_5, the NO concentration was determined from a least squares fit of the sample spectrum to that of the reference. The N_2O_5 concentration was determined from the change in the NO concentration from the reference value. The TDLAS response for H_2O vapor was periodically calibrated by diverting the flow from the humidifier past the flow reactor and directly into the White cell. For these calibrations, high H_2O concentrations were generated by the humidifier. These could then be determined accurately from the humidifier temperature and pressure. Since this procedure was too time consuming for daily use, routine H_2O vapor calibrations were made relative to the NO response. The responsivity ratio between NO and H_2O vapor was acquired each time the full H_2O vapor calibration was carried out. As long as the laser power is measured for both lines and the same conditions of pressure and modulation are employed, this ratio remains constant. Its value was used together with the daily NO calibration to make a daily H_2O vapor calibration.

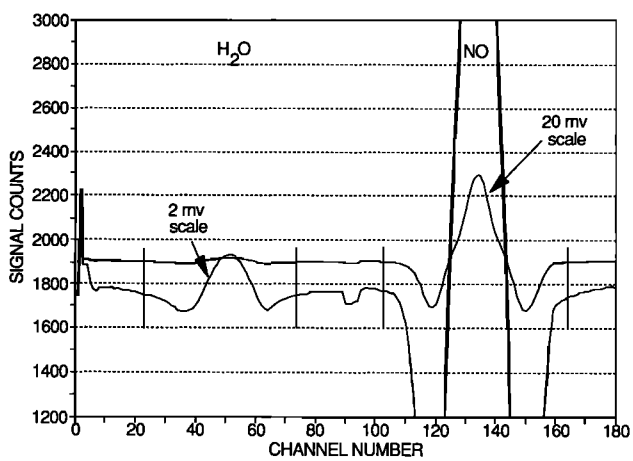

Fig. 4. Typical H_2O and NO data acquired from a tunable diode laser absorption spectroscopy scan averaged for 20 s. The H_2O feature on the left occurs at 1816.0589 cm^{-1}, and the NO doublet on the right occurs at 1816.5455 cm^{-1}. The structure at channels 90-95 reflects the jump in the laser current which is required to access both features in the same scan. The portions fit to reference spectra are indicated by the vertical lines. The scale used for the determination of H_2O vapor (7 ppmv) was 10 times as sensitive as that used for NO (580 ppbv).

DATA REDUCTION

Mass Transport and Heterogeneous Reactions

The principles of reactions in small droplets have been described by *Schwartz and Freiberg* [1981] and *Schwartz* [1986]. We can apply these principles to the present laboratory measurements as follows. We assume that N_2O_5 undergoes a pseudo first-order reaction within the liquid phase of the aerosol. The rate of change of the gas-phase N_2O_5 concentration may be expressed in terms of a second-order rate constant k_A as

$$\frac{d[N_2O_5(g)]}{dt} = -k_A\,[N_2O_5(g)]\,N_p, \tag{7}$$

where N_P is the number density of aerosol particles. Loss of N_2O_5 at the walls gives rise to an additional term, as will be discussed later. The gas-phase loss of N_2O_5 with H_2O is over 5 orders of magnitude slower than the heterogeneous loss and thus is omitted from consideration here.

In the limit where the surface of the particles is in equilibrium with the gas phase (i.e., the rate of mass transport from the gas phase to the liquid phase is much faster than the rate of the liquid-phase reaction), we have $k_A \approx k_L$, where

$$k_L = 4\pi a^3 H(N_2O_5) k_R \left(\frac{q\coth q - 1}{q^2}\right) \tag{8}$$

[*Schwartz and Freiberg*, 1981; *Schwartz*, 1986]. Here a is the particle radius, $H(N_2O_5)$ is the dimensionless Henry's law constant, k_R is the pseudo first-order rate constant for the liquid-phase reaction, q is a reaction-diffusion parameter defined by

$$q = a\sqrt{\frac{k_R}{D_L}}, \tag{9}$$

and D_L is the liquid-phase diffusion coefficient. When q is small, diffusion is fast enough to keep the drop well mixed; then the quantity in parentheses in (8) approaches 1/3, and k_L is proportional to a^3. When q is large, essentially all of the reaction occurs in a thin layer of liquid near the surface; then the quantity in parentheses in (8) reduces to $1/q$, and k_L is proportional to a^2.

In the limit where the rate of liquid-phase reaction is so fast that the overall rate is controlled by the rate of mass transport from the gas phase to the liquid phase, we have $k_A \approx k_G$, where

$$k_G = \frac{\alpha\pi a^2 \langle v\rangle}{1+\dfrac{3\alpha(1+0.37Kn)}{4Kn(1+Kn)}} \tag{10}$$

[*Fuchs and Sutugin*, 1970]. Here α is the mass accommodation coefficient, $\langle v\rangle$ is the mean molecular velocity of N_2O_5, and Kn is the Knudsen number defined by

$$Kn = \frac{3D_G}{a\langle v\rangle}, \tag{11}$$

where D_G is the gas-phase diffusion coefficient. When Kn is large compared to α, (10) reduces to the molecular kinetic theory result ($\alpha\pi a^2\langle v\rangle$) and when Kn is small, (10) yields the

result for diffusion in a continuous fluid ($4\pi D_G a$). In the present experiments, Kn falls in the range of 1 to 4, and our results approximate the kinetic theory limit with corrections of the order of 1 to 5%.

In the general case in which the rates of gas-phase mass transport and liquid-phase reaction and diffusion are comparable, we have

$$\frac{1}{k_A} = \frac{1}{k_G} + \frac{1}{k_L} \tag{12}$$

[*Schwartz*, 1986]. This may be obtained by equating the reactive flux in the liquid phase to the flux for mass transfer to the drop.

It is common to combine liquid-phase reaction and diffusion into a reaction probability γ. In this case we replace α in (10) with γ and obtain

$$k_A = \frac{\gamma \pi a^2 \langle v \rangle}{1 + \dfrac{3\gamma\,(1+0.37Kn)}{4Kn(1+Kn)}} . \tag{13}$$

By comparing this with (12), we see that the value of γ obtained from (13) will be independent of the drop radius only if either $k_L >> k_G$ (so that $\gamma \approx \alpha$) or k_L is proportional to the square of the drop radius. This latter condition will be met when $q >> 1$. Since q is proportional to drop radius, this condition will be met only for drops greater than some minimum size; it will always be met on bulk surfaces. In the absence of a detailed knowledge of the parameters that determine k_L, the size below which γ depends on particle size cannot be calculated with certainty. One objective of the present study is to determine whether γ is constant over the range of particle sizes that we can work with.

Reaction Probability Measurements

For each temperature and relative humidity, N_2O_5 decays were measured for several particle sizes and number densities. For each decay the N_2O_5 concentration was measured for a series of injector positions. The flow will be disturbed for some distance downstream of the injector. The distance required for fully laminar flow to develop was calculated from the formula for the inlet length [*Langhaar*, 1942]

$$L_l = 0.0732 Q_V \frac{\rho}{\eta}, \tag{14}$$

where Q_V is the volumetric flow rate, ρ is density, and η is viscosity. No data points were taken within this inlet length.

The injector positions were initially converted to reaction times using the plug flow approximation. Each decay was fit to an exponential using an unweighted nonlinear regression to obtain an "observed" first-order decay rate. Representative decays are shown in Figure 5 for three different aerosol surface areas. Each determination of γ included decays for which no particles were present as well as decays with a variety of particle sizes and number densities. The observed decay rates depend on both the reaction with the aerosol and the reaction on the flow reactor walls; in high-pressure flows the observed decay rate is not simply a linear sum of the two contributions [*Brown*, 1978]. The observed decay rate is the smallest eigenvalue of the continuity (or reaction-diffusion) equation. For a pseudo first-order reaction in fully developed laminar flow, this equation is

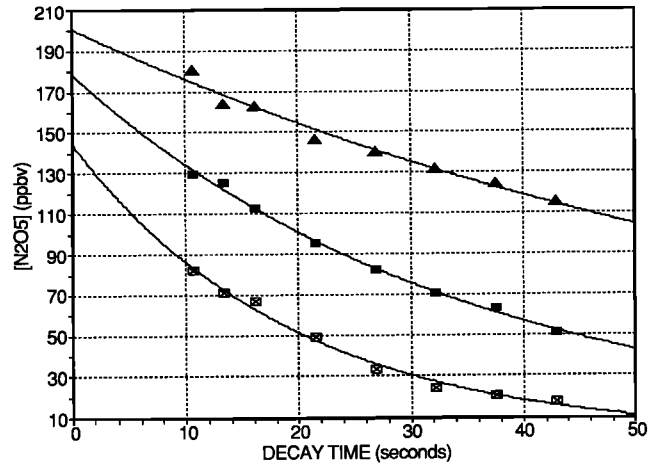

Fig. 5. Representative decay curves in the absence of aerosol (solid triangles) and for aerosol surface areas of 2711 (solid boxes) and 6850 (boxes with crosses) $\mu m^2\ cm^{-3}$. The curves are the results of exponential fits. The conditions for this experiment were 260 K, 709 mbar, 69.7% H_2SO_4 by weight, 3.1% relative humidity, 98.5 ppmv H_2O, and an initial N_2O_5 mixing ratio of 187 ppbv.

$$k_A N_P [N_2O_5] = -2\langle U \rangle \left(1 - \left(\frac{r}{R}\right)^2\right) \frac{\partial [N_2O_5]}{\partial Z} + \frac{D_G}{r}\frac{\partial}{\partial r}\left(r \frac{\partial [N_2O_5]}{\partial r}\right) + D_G \frac{\partial^2 [N_2O_5]}{\partial Z^2}, \tag{15}$$

where r is the radial distance from the center of the flow tube, R is the tube radius, $\langle U \rangle$ is the plug flow velocity, and Z is the axial distance from the inlet of the reactor. Equation (15) must be solved subject to the appropriate boundary condition for reaction on the flow reactor wall [*Murphy and Fahey*, 1987],

$$\frac{\gamma_W \langle v \rangle}{4} [N_2O_5] = -D_G \frac{\partial [N_2O_5]}{\partial r} \quad \text{at } r = R, \tag{16}$$

where γ_W is the reaction probability on the wall.

For the decays at each temperature and relative humidity, an unweighted nonlinear regression was used to determine γ and γ_W. For each successive estimate of these parameters, the numerical method of *Brown* [1978] was used to obtain the eigenvalues of (15) for each decay. The axial diffusion term, the last term in (15) was accounted for by replacing $k_A N_P$ in (15) with

$$K_A N_P - \frac{\beta^2 D_G}{\langle U \rangle^2}, \tag{17}$$

where β is the computed eigenvalue corresponding to the observed decay rate. This corresponds to making the substitution

$$D_G \frac{\partial^2 [N_2O_5]}{\partial Z^2} = D_G \frac{\partial^2}{\partial Z^2}\left([N_2O_5]_o e^{-\beta t}\right) = \frac{D_G \beta^2}{\langle U \rangle^2} [N_2O_5], \tag{18}$$

in (15). The use of (17) is valid as long as the axial diffusion correction is not too large; it did not exceed 10% in these experiments. This correction was recomputed at each stage of the iterative eigenvalue calculation. Values γ and γ_W were varied

to find the eigenvalues that provided the best fit of the observed decay rates. In addition to the particle surface area, the decay rates depend weakly on the pressure (through D_G), the particle size (through *Kn* in equations (11) and (13)), and the flow velocity (equation (17)). A typical plot of observed and calculated decay rates as function of aerosol surface area is shown in Figure 6. Calculations were carried out for two different particle diameters (0.060- and 0.250-μm) to show the small dependence of decay rate with particle size.

For high-pressure flows the actual reaction times are less than those computed from a plug flow approximation, since both the flow velocity and the reactant concentration are higher at the center of the flow tube than at the walls. This is accounted for in solving the continuity equation; the correction factor can be as large as 1.6 [*Brown*, 1978]. In this work we found typical correction factors of 1.05 to 1.15, although some were as high as 1.4. In previous work, *Mozurkewich and Calvert* [1988] had assumed a correction factor of 1.3 ± 0.3. Since their conditions were similar to those of the present work, the reaction probabilities reported there should probably be lowered by about 15%.

Equation (13) was used to account for the effects of diffusion on k_A; diffusion usually reduced k_A by less than 2%. The value of the N_2O_5 diffusion coefficient in air D_G was estimated by the method of Hirschfelder [*Reid and Sherwood*, 1966, pp. 523-526] with Lennard-Jones parameters for N_2O_5 taken from work by *Patrick and Golden* [1983]. The resulting expression is

$$D_G = \left(0.0854\, cm^2\, s^{-1}\right)\left(\frac{T}{273.15\ K}\right)^{1.95}\left(\frac{1.00\ bar}{P}\right). \quad (19)$$

Since this diffusion coefficient is involved only in making relatively small corrections, the results will not be sensitive to the exact value used. A 20% uncertainty in the diffusion coefficient causes only a 5% uncertainty in γ.

Results and Discussion

Data were acquired for aerosol compositions of 54 to 82 wt % H_2SO_4 at temperatures from 225 K to 293 K. The flow reactor pressure, flow velocity, and N_2O_5 mixing ratio were varied to detect possible systematic errors. We observed no correlations between γ and any of these parameters. The reaction probability was determined at each temperature and aerosol composition as discussed in the previous section. In any given set of experiments, the aerosol diameter was typically varied from 0.1- to 0.2-μm; in some experiments the range was 0.06- to 0.25 μm.

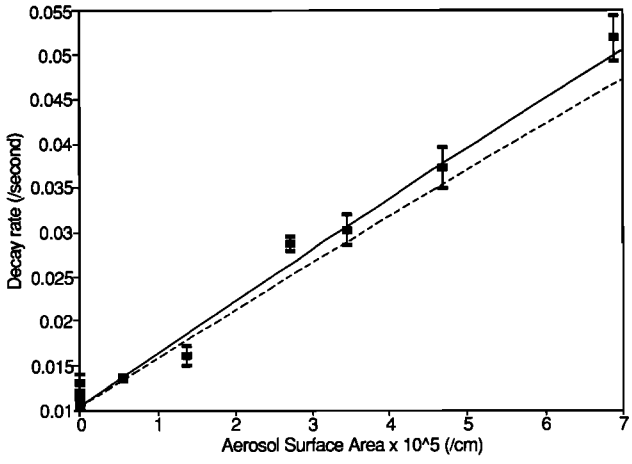

Fig. 6. A representative plot of the observed plug flow decay rate (points) and calculated rate (lines) as a function of aerosol surface area. Curves are plotted for particle diameters of 0.060 μm (solid curve) and 0.250 μm (broken curve) to show the small dependence of decay rate on particle size due to gas-phase diffusion. The calculated rates use the best-fit values of the reaction probability on the flow reactor walls (2.68 x 10^{-6}) and on the particles (0.1169). The experimental conditions are the same as for Figure 5.

At high relative humidities, particularly at low temperatures, substantial deviations from the expected behavior were observed. Under these conditions the wall rate would sometimes gradually increase over the time required to measure a series of decays with different aerosol concentrations. High aerosol number density and/or surface areas appear to enhance this phenomenon. Under these conditions, measurements had to be broken down into small groups of decays so that the wall loss rate was approximately constant within each group.

The conditions that produced the increasing wall loss rates would sometimes lead to an apparent increase, by as much as a factor of 5 in the reaction probability on the particles. This increase in γ was generally accompanied by wall loss rates greater than 0.025 s^{-1}, deviations from exponential decay for longer reaction times, and high values of the N_2O_5 concentrations at the inlet as extrapolated from the exponential decay. These effects seem to be caused by NO production as a result of reactions on the flow reactor walls. Since the N_2O_5 concentration is determined by the amount of NO consumed, such production of NO on the flow reactor walls leads to an apparent faster rate.

We observed this NO production directly in experiments conducted at 247 K with N_2O_5 concentrations around 100 ppbv, a fixed injector position of 85 cm, and aerosol number densities of about 4.7 x 10^4 particles cm^{-3}; this was high enough to consume most of the N_2O_5. After exposing the walls for 5 hours, this procedure caused the production of 15 to 20 ppbv of NO in addition to the NO added to the converter. After turning off the supply of N_2O_5, the artifact NO disappeared in approximately 140 min. Reintroduction of N_2O_5 caused the reappearance of the artifact NO, also in approximately 140 min. This time scale is consistent with the time scales observed for changes in γ during the experiments. We believe that NO_2 (either present as an impurity in the N_2O_5 or produced by its decomposition) reacts with water on the flow reactor walls to produce HONO and/or HNO_3. The NO may then come from decomposition of the HONO, possibly in the thermal converter.

Results that gave indications of artifact NO production have been eliminated from our final tabulations. After recognizing the existence of this artifact, its prevalence was reduced considerably by working with low aerosol number densities, especially for lower temperatures. At temperatures around 230 K, for example, this required that number densities be kept below 20,000 particles cm^{-3}. When working at low temperatures under very dry conditions (4 ppmv H_2O at 230 K), high γ values were occasionally obtained. Although we have not managed to establish the cause of this, one possibility is that not all of the SO_3 is reacting in the particle source. This could then lead to growth of the particles after size selection by the DMA. However, repeated measurements made the occurrence of this problem obvious.

The results of these measurements are summarized in Table 2 and Figures 7-10. Mean γ values were determined at each

TABLE 2. Summary of Measured Reaction Probabilities γ at Various Experimental Conditions

Temperature, K	P, (mbar)	RH, %	H_2SO_4, wt %	Diameter, μm	γ	1σ
293	820	0.19	83.6	0.11-0.17	0.076	0.009
293	764	0.22	82.5	0.12-0.19	0.042	0.016
293	500	0.73	78.7	0.12-0.18	0.063	0.015
273	625	9.70	64.0	0.09-0.15	0.116	0.017
273	589	7.38	65.3	0.06-0.11	0.097*	0.011
273	583	3.34	70.3	0.06-0.18	0.094*	0.007
273	753	2.04	73.0	0.09-0.15	0.109	0.014
273	776	2.05	73.0	0.11-0.16	0.045†	0.015
273	811	2.01	73.1	0.06-0.14	0.100†	0.010
273	812	1.91	73.3	0.09-0.13	0.045†	0.009
273	589	1.72	73.5	0.06-0.13	0.071†	0.004
273	760	1.57	74.0	0.11-0.16	0.081†	0.004
273	803	0.89	76.1	0.09-0.13	0.109†	0.014
273	747	0.61	78.4	0.08-0.14	0.095	0.007
273	580	0.60	78.5	0.08-0.16	0.109	0.008
273	704	0.54	78.8	0.11-0.17	0.112	0.012
273	569	0.43	79.5	0.09-0.14	0.099	0.006
273	521	0.31	80.5	0.09-0.14	0.099	0.010
273	536	0.23	81.4	0.06-0.16	0.103	0.013
260	695	17.9	56.6	0.12-0.16	0.126	0.008
260	736	9.37	62.7	0.08-0.19	0.104	0.020
260	709	3.14	69.7	0.09-0.23	0.117	0.005
260	700	1.71	73.4	0.07-0.18	0.155	0.014
260	713	0.98	75.2	0.09-0.15	0.110	0.010
260	711	0.94	75.5	0.06-0.15	0.111	0.020
260	692	0.78	76.2	0.10-0.21	0.115	0.009
260	749	0.53	77.6	0.08-0.18	0.041†	0.007
260	707	0.52	77.8	0.07-0.18	0.180†	0.008
260	675	0.52	78.5	0.10-0.21	0.049†	0.002
247	712	6.85	64.3	0.13	0.179	0.033
247	781	4.07	67.6	0.07-0.20	0.182	0.023
247	683	1.18	73.9	0.10-0.17	0.153	0.014
247	767	4.39	67.2	0.10-0.20	0.131	0.007
247	720	3.03	68.3	0.14-0.16	0.136	0.025
247	717	2.97	69.9	0.14-0.19	0.118	0.028
247	716	1.58	72.4	0.13-0.19	0.145	0.035
247	776	0.90	74.6	0.11-0.17	0.154	0.019
247	776	0.65	76.0	0.11-0.17	0.143	0.009
247	777	1.35	73.1	0.11-0.17	0.156	0.015
247	763	9.33	61.8	0.10-0.17	0.090	0.010
247	764	4.99	65.5	0.12-0.17	0.152	0.017
247	756	3.07	69.1	0.12-0.17	0.124	0.032
247	745	7.75	63.2	0.11-0.15	0.150	0.026
247	748	9.00	62.1	0.10-0.13	0.083	0.039
247	748	10.4	60.7	0.12-0.14	0.084	0.020
225	449	17.6	54.0	0.15-0.22	0.087	0.027
230	673	12.4	58.0	0.10-0.15	0.083	0.054
231	668	6.4	63.4	0.09-0.18	0.079	0.005
230	512	6.0	63.7	0.07-0.14	0.060	0.020
231	679	3.7	67.0	0.09-0.14	0.111	0.020
234	504	5.6	64.5	0.09-0.10	0.100	0.035
234	499	3.2	68.0	0.10-0.13	0.094	0.034
234	499	2.9	68.6	0.08-0.17	0.134	0.046
231	489	2.9	68.6	0.09-0.19	0.104	0.014
231	307	1.8	70.6	0.08-0.21	0.131	0.051
230	387	1.7	70.9	0.08-0.20	0.179	0.036
234	497	1.8	70.9	0.09-0.23	0.138	0.024

*Measurements in the presence of CH_2O.

†Points excluded from the averages given in Table 3.

temperature; these are summarized in Table 3. Unless otherwise stated, all error limits cited in the following discussion are 95% confidence intervals obtained from the product of the standard error and the appropriate Student t factor. Based on uncertainties in the flow reactor diameter, mass flow rate, and N_2O_5 diffusion coefficient, we estimate a total maximum systematic error of ±13% for all determinations. Of course, unknown systematic errors from uncorrectable wall loss variations during our aerosol decays would make the true systematic error larger than this estimate. A total uncertainty

TABLE 3. Summary of Reaction Probability Determinations at Various Temperatures

Temperature, K	Composition (H_2SO_4, wt %)	Reaction Probability	Number of Determinations
293	78.7-83.6	0.06 ± 0.04	3
273	64.0-81.4	0.103 ± 0.006	10
260	56.6-76.2	0.120 ± 0.016	7
247	60.7-62.1	0.086 ± 0.009	3
247	63.2-76.0	0.148 ± 0.011	13
230-234	68.6-70.9	0.146 ± 0.036	4
231-234	64.5-68.6	0.102 ± 0.011	4
225-231	54.0-63.7	0.077 ± 0.019	4

The error estimates given are 95% confidence intervals; these reflect the random error. The total uncertainty is obtained by algebraic addition of a 13% systematic error to each error estimate.

was obtained from addition of the 95% confidence interval and the estimated systematic error.

Limited data at 293 K were acquired for a comparison with the previous results of *Mozurkewich and Calvert* [1988]. Our mean value of 0.06 is somewhat lower than the previous value of 0.10. As discussed in the data reduction section, the earlier result is probably high by about 15%. Similarly, at 273 K our result of 0.10 is somewhat lower than the value of 0.14 reported by Mozurkewich and Calvert. In both cases, the uncertainty limits overlap.

Results at 273 K are shown in Figure 7. With the exception of H_2SO_4 compositions around 73.1% by weight (corresponding to a H_2O:H_2SO_4 mole ratio of 2:1), Figure 7 shows that γ is composition independent. At compositions around 73.1%, low values of γ were sometimes obtained. It is possible but not likely that these low values of γ are due to scatter in the data, or they may result from a real effect at this composition. However, at the time these measurements were made, we were having difficulty with our air supply such that the zero air contained large quantities of water and carbon dioxide; these were due to oxidation of hydrocarbons in the compressed air supplied to the clean-air generator. It is possible that at that time the zero air also contained organics which may have altered the aerosol reactivity. Excluding the data points where the air supply may have been contaminated, we obtain an average γ value of 0.103 ± 0.006 at 273 K.

High concentrations of formaldehyde did not affect γ. Formaldehyde was inadvertently produced in some experiments by reaction of H_2SO_4 with the Delrin seats in the DMA outlet valves and was observed with our TDLAS using an IR feature near the 1816.5 cm^{-1} NO line. Experiments at 65.3 and 70.3% composition at 273 K were acquired in the presence of 3 to 19 ppmv CH_2O; these suggest that stratospheric CH_2O should not affect the reaction between N_2O_5 and H_2SO_4 aerosol.

Results at 260 K are displayed in Figure 8. There is no apparent dependence of γ with composition below 77.4%. There is a great deal of scatter for the three measurements above this value. At this temperature and composition, the stable condensed phase is solid H_2SO_4•H_2O [*Gable et al.*, 1950]. This raises the possibility that the high value results from a supercooled liquid aerosol and that the two low values are for an aerosol in which some or all of the particles are frozen. In these experiments we have no way of determining the phase of the particles. The present data are insufficient to prove that these observations are not a result of some unknown systematic bias. The average value of 0.120 ± 0.016 given in Table 3 is based on the seven points with compositions below 77.4% H_2SO_4. Averaging all 10 points yields γ = 0.111 ± 0.030. The average of the two low values at about 78% H_2SO_4 is 0.045.

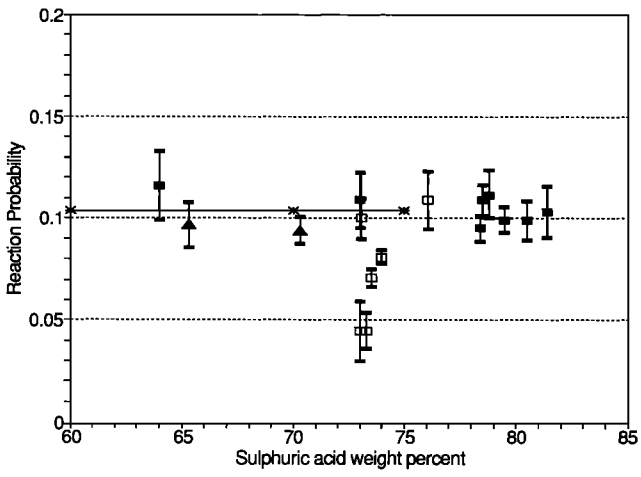

Fig. 7. Summary of results at 273 K. Open boxes, points that were dropped from the average because of possible organic contaminants in the air supply; solid triangles, measurements in the presence of CH_2O; asterisks, points calculated from the semiempirical theory presented in the text. The error bars represent 1 standard deviation of each determination.

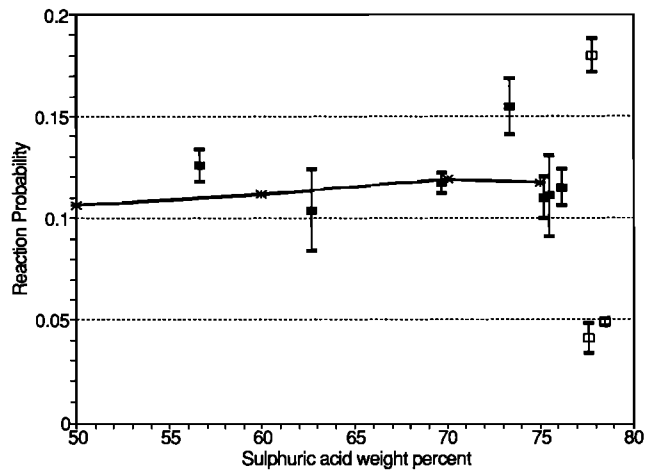

Fig. 8. Summary of results at 260 K. Solid boxes, points that were included in the average; open boxes, points that were excluded from the average; asterisks, points calculated from the semiempirical theory. The error bars represent 1 standard deviation of each determination.

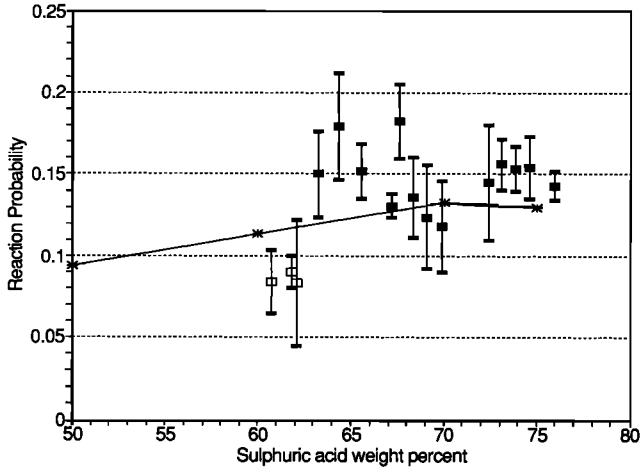

Fig. 9. Summary of results at 247 K. Solid boxes measured values for compositions of >63% H_2SO_4; open boxes, measured values for compositions of <63% H_2SO_4; asterisks, points calculated from the semiempirical theory. The error bars represent 1 standard deviation of each determination.

As can be seen in Figure 9, at 247 K there is no composition dependence for 63% to 76% H_2SO_4. The 13 points in this range result in an average γ of 0.148 ± 0.011. The three data points below 63% result in an average γ of 0.086 ± 0.009. Thus γ seems to increase abruptly by a factor of 1.7 ± 0.2 at 63% H_2SO_4. It is interesting to note that $H_2SO_4 \cdot 4H_2O$ (57.7% H_2SO_4) has a melting point of 244.8 K [*Gable et al.*, 1950], just below the temperature of these measurements. At 247 K, the stable condensed-phase $H_2SO_4 \cdot H_2O$ may exist for compositions of >75.4% [*Gable et al.*, 1950]. Our one measurement in this region (76% composition) does not show a drop in γ, suggesting that the aerosol was a supercooled liquid.

Data for 225 K to 234 K are shown in Figure 10; these data are grouped together, since the temperatures are close together and any temperature dependence is weak. The correlation coefficient between γ and composition is 0.46; this is statistically significant at the 90% confidence level. To facilitate comparison with other temperatures, we have divided the data into three groups, as shown in Table 3. For all but the three highest composition points at 234 K, the stable phase is one of the solid hydrates: $H_2SO_4 \cdot 2H_2O$, $H_2SO_4 \cdot 3H_2O$, or $H_2SO_4 \cdot 4H_2O$. In these cases there is again the possibility that some or all the particles may be frozen. The temperature dependence of γ for various composition surfaces is shown in Figure 11. As can be seen, our data show that γ decreases as temperature increases above 247 K. However, below 247 K, the temperature dependence appears to level off and, at lower H_2SO_4 compositions, to reverse (Figure 11*c*). The result is that γ appears to depend on composition at the lower temperatures. This is in contrast to the results of *Hanson and Ravishankara* [1991] who found no dependence on temperature or composition at these lower temperatures. However, the average value of 0.108 for all our measurements near 230 K is in agreement with the results of Hanson and Ravishankara. In

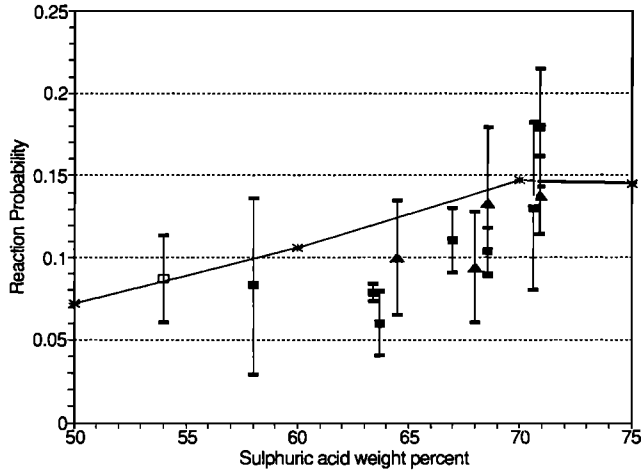

Fig. 10. Summary of results at 225 K (open boxes), 230 K (solid boxes), and 234 K (solid triangles). Asterisks indicate points calculated from the semiempirical theory for 230 K. The error bars represent 1 standard deviation of each determination.

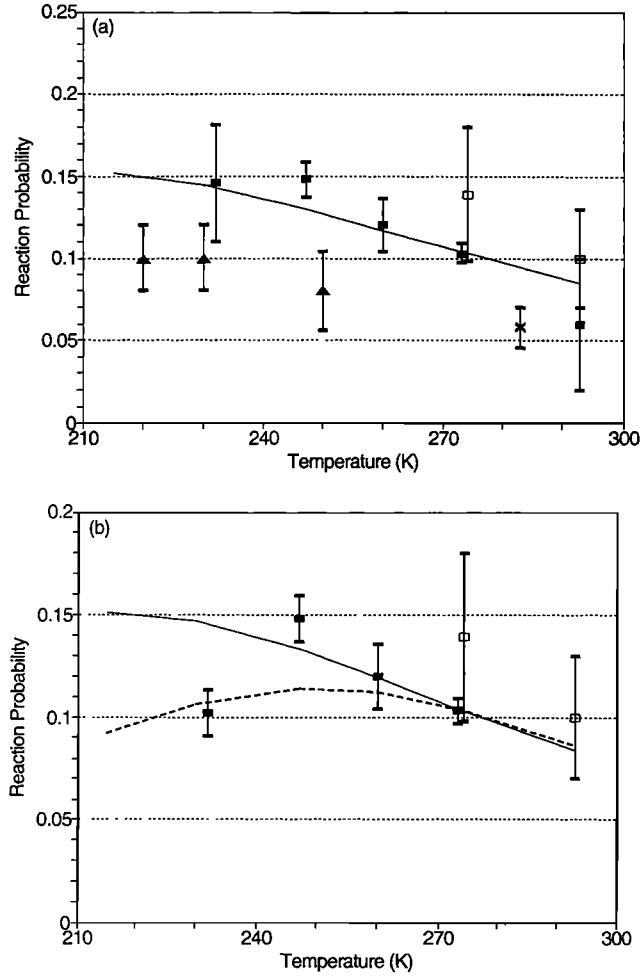

Fig. 11. Summary of reaction probabilities for N_2O_5 on H_2SO_4/H_2O surfaces: (*a*) >69% H_2SO_4; (*b*) 64 to 68% H_2SO_4; (*c*) 54 to 64% H_2SO_4. Values are taken from this work (solid boxes); *Mozurkewich and Calvert* [1988] (open boxes); *Hanson and Ravishankara* [1991] (solid triangles); and *Van Doren et al.* [1991] (crosses). With the exception of this work, the error bars represent the total uncertainty of the respective study. In this study these error bars give the measurement imprecision at the 95% confidence interval (see Table 3). Our total uncertainty is obtained by algebraic addition of a 13% systematic estimate to these estimates. The curves are calculated from the semiempirical theory given in the text for compositions of 70 and 75% H_2SO_4 (solid curve), 60% H_2SO_4 (dashed curve), and 50% H_2SO_4 (dotted curve).

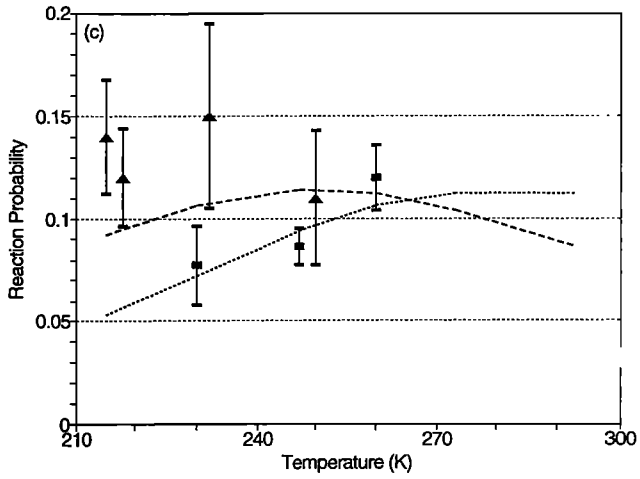

Fig. 11. (continued)

addition to the data shown in Figure 11, *Golden et al.* [1993] report a composition- and temperature-independent lower bound to γ of 0.06.

Because the change in the temperature dependence of γ occurs near the freezing points of the solutions, one must consider the possibility that the change is due to freezing of the aerosol particles. One argument against this is that in the absence of ice nuclei, small aerosol particles have a pronounced tendency to supercool; in fact, stratospheric particles do not generally freeze even though they have lifetimes of many months [*Turco et al.*, 1982]. Also, our results at the lower temperatures are comparable to the results obtained by *Hanson and Ravishankara* [1991] for a supercooled liquid surface. In the following section, we provide a theoretical framework for understanding the observed temperature and composition dependencies. This theory, however, does not explain the two low γ values measured at 260 K for H_2SO_4 compositions greater than 77%.

Theoretical Interpretation

The usual analysis of gas-liquid reaction rates is based on equations (8) through (12). We find that the measured reaction probabilities do not depend on particle size; this implies that q (equation (9)) is very large. In this limit, substituting (8) and (10) into (12) and assuming that $\alpha << Kn$, we obtain

$$\frac{1}{\gamma} = \frac{1}{\alpha} + \frac{<v>}{4H\sqrt{k_R D_L}}. \tag{20}$$

The mass accommodation coefficient α is the fraction of N_2O_5 molecules which become trapped in the potential well for adsorption. Since energy transfer in collisions of a gas molecule with a liquid surface is very efficient [*Fuchs*, 1964, pp. 21-29], we expect α to be near unity as long as the well depth is at least a few times kT [*Mozurkewich*, 1986]. We estimate the Henry's law constant for N_2O_5 by the method of *Berdnikov and Bazhin* [1970] (6 to 60 over the range 273 to 230 K) and the diffusion coefficient by the method of *Reid and Sherwood* [1966, p. 550]. With these estimates, setting γ equal to 0.12 in (20) yields estimated values of k_R ranging from 4 x 10^8 s^{-1} (40% H_2SO_4 at 230 K) to 7 x 10^{10} s^{-1} (80% H_2SO_4 at 273 K). This implies that the rms distance that a N_2O_5 molecule can diffuse into the liquid ranges from 0.03 to 0.4 nm. Since these are of the order of molecular dimensions or less, we draw the conclusion that solvation and reaction are not distinct steps as was assumed in deriving (20).

In light of these results, we propose that the reaction proceeds in two steps: the physical adsorption of an N_2O_5 molecule onto the surface and the solvation of this adsorbed molecule accompanied by an almost simultaneous conversion into dissolved NO_3^- or HNO_3. The reaction probably is determined by the competition between the second step and desorption from the surface. Let k_D be the rate of desorption and k_S be the rate of reaction on the surface; then we have for the reaction probability

$$\gamma = \frac{k_S}{k_S + k_D}. \tag{21}$$

This has the same functional form as that suggested by *Jayne et al.* [1991] for the uptake of alcohols and organic acids by water drops. In that case, k_S is replaced by the rate of physical solvation of the condensing molecule.

Davidovits et al. [1991] have presented a model for estimating k_S in which the solvation of the condensing gas molecule is due to water molecules condensing onto it. It is difficult to see how this model could reproduce the observed lack of dependence of γ on aerosol composition and therefore H_2O partial pressure. Here we offer an alternative explanation that shows how the physical properties of the solution could lead to the observed temperature and composition dependence.

In this model we assume that the rate of desorption, k_D in (21) is independent of composition and has a temperature dependence given by

$$K_D = A_D \exp\left(-\frac{E_{act}}{RT}\right). \tag{22}$$

We also assume that the solvation rate k_S is proportional to the rate at which "holes" are formed at the surface of the liquid. This amounts to assuming that the molecule becomes solvated when a sufficiently large hole forms below it, thus allowing the N_2O_5 molecule to enter the liquid phase. At equilibrium, the rate at which holes form at the surface must be equal to the rate at which they diffuse to the surface from the interior of the liquid [*Frenkel*, 1955]. Thus it is reasonable to assume that k_S is proportional to both the number density of holes N_H and the diffusion coefficient of the holes D_H.

Assuming that the macroscopic surface tension σ of the liquid may be used to calculate the energy required to form a hole of radius r, we have [*Frenkel*, 1955]

$$N_H = (\text{constant}) \exp\left(\frac{-4\pi r^2 \sigma}{kT}\right). \tag{23}$$

The hole diffusion coefficient may be estimated by the Stokes-Einstein relation:

$$D_H = \frac{kT}{6\pi r \eta}. \tag{24}$$

Now we may rearrange (21) and make use of (22) through (24) to obtain

$$\frac{\gamma}{1-\gamma} = \frac{k_S}{k_D} = G \exp\left(\frac{E_{act}}{RT}\right)\left(\frac{T}{\eta}\right)\exp\left(\frac{-4\pi r^2 \sigma}{kT}\right), \tag{25}$$

where G is a constant.

We have applied (25) to our data as follows. First, the viscosities for H_2SO_4/H_2O solutions [*Washburn*, 1928] were fit to equations of the form [*Reid and Sherwood*, 1966]

$$\ln(\eta) = A + \frac{B}{T} + \frac{C}{T^2}, \quad (26)$$

so that the data could be extrapolated to the temperatures of these experiments. Next, the solution surface tensions were calculated from

$$\sigma = \sigma_o + bT, \quad (27)$$

with coefficients for the desired compositions interpolated from the results of *Sabinina and Terpugow* [1935]. The hole radius r was set equal to 0.317-nm (a few percent larger than implied by the estimated N_2O_5 molal volume of 72 cm^3 mol^{-1}); with this choice, the predicted γ is independent of composition for 60% to 75% H_2SO_4 at 273 K. The values of G and E_{act} were then chosen so as to give γ=0.104 at 273 K and a reasonable temperature dependence. E_{act} was adjusted by eye; a least squares fit was not used because of the relatively few temperatures at which γ was measured and the few compositions for which viscosity data are available. The values chosen for the coefficients were E_{act} = 94.5 kJ/mol and $G = 5.46 \times 10^{-10}$ cp K^{-1}. This value of E_{act} is 3.4 times higher than one would expect based on the Henry's law constants given above. This calculation, however, yields the heat of solution, which represents a lower limit for the activation energy. In addition, the Henry's law constants given estimated above are uncertain by at least a factor of 10.

The curves resulting from this model are shown in Figures 7 through 11; these reproduce the essential features of the data. In particular, it should be noted that although the same value of E_{act} is used for all compositions, the calculated temperature dependencies are not the same for all compositions. At 273 K, σ decreases with increasing H_2SO_4 concentration, while η increases. As a result, the effects of these two quantities on k_S cancel. However, since these quantities have different temperature dependencies, the cancellation is not as effective at other temperatures. As a result, a composition dependence appears at 230 K even though there is no such dependence at 273 K.

The principle disagreement between the measured and calculated values for γ occurs for compositions around 60% H_2SO_4 (dashed curve in Figure 11*c*). The calculated values do not drop off as rapidly as the measured values at low temperatures. It must be emphasized that both the surface tension and the viscosity values employed here were obtained from large extrapolations at temperatures above 273 K. It is entirely possible that the calculated surface tensions and viscosities underpredict the true values around 230 K. This, in turn, would lead to an overprediction of γ by (25). The agreement of this semiempirical theory with the results of *Hanson and Ravishakara* [1991] is not as good. This could be due to the even larger extrapolation which is required to reach their experimental temperatures around 215 K.

TABLE 4. Extrapolated Reaction Probabilities for H_2SO_4 Aerosol as a Function of Altitude at Three Different Latitudes Spanning Two Seasons

Altitude, km	Pressure, mbar	Temperature, K	$[H_2O]$, ppm	Composition (H_2SO_4, wt %)	γ
		January, 85°N			
15	119	206	2.6	64	0.10
20	58	198	3.0	60	0.06
25	28	194	3.7	59	0.05
30	14	195	4.5	63	0.08
35	7	200	4.9	71	0.15
40	3	209	5.1	78	0.15
		January, 45°N			
15	119	213	2.3	70	0.15
20	58	207	2.4	69	0.15
25	28	208	2.8	73	0.15
30	14	213	3.4	77	0.15
35	7	222	4.0	82	—
40	3	233	4.6	88	—
		July, 45°N			
15	119	216	2.3	72	0.15
20	58	213	2.3	73	0.15
25	28	217	2.7	77	0.15
30	14	229	3.2	83	—
35	7	241	3.8	89	—
40	3	256	4.4	90	—
		July, 85°S			
15	119	197	2.6	54	0.04
20	58	192	2.1	54	0.03
25	28	189	2.6	54	0.03
30	14	190	4.4	57	0.03
35	7	197	4.8	69	0.13
40	3	207	4.9	77	0.15

Results are based on our semiempirical theory. Temperature, pressure, and water vapor mixing ratio profiles were calculated using the model described by *Granier and Brasseur* [1992]. The aerosol composition was calculated from work by *Gmitro and Vermeulen* [1964]. Blanks indicate that γ could not be calculated at the indicated composition from the available data.

CONCLUSIONS

The reaction probabilities γ observed in this study are comparable to other recently published results [*Hanson and Ravishankara*, 1991; *Mozurkewich and Calvert*, 1988, *Van Doren et al.*, 1991]. However, the present study reveals dependencies on both temperature and composition. At temperatures above 247 K, γ increases as the temperature decreases, and there is no dependence of γ on composition within the range that we investigated. As the temperature decreases below 247 K, γ levels out for particle compositions near 70% H_2SO_4 by weight and begins to decrease for compositions near 60% H_2SO_4 by weight. As a result, there appears to be a composition dependence at 230 K.

We observed that γ does not depend on particle size; this is consistent with the fact that our measurements on small particles give about the same γ as measurements on bulk surfaces. Formaldehyde concentrations as high as 19 ppmv also did not affect γ. Considering the limited solubility of N_2O_5, the relatively large values of γ imply that the liquid-phase reaction is very fast; this in turn implies that N_2O_5 does not penetrate more than a few tenths of a nanometer into the liquid phase. Thus we conclude that the processes of solvation and liquid-phase reaction are not independent. We found that a simple physical model based on the hole theory of the liquids can reproduce the general trends in composition and temperature that we have observed for all but the highest acid concentrations at 260 K. Here, we cannot rule out the possibility that some of the aerosol particles may be frozen.

This semiempirical theory can be used to extend our γ determinations to cover lower stratospheric temperatures than those studied here. As shown in Table 4, stratospheric temperatures can attain values as low as 189 K, and our theory indicates that γ should decrease from its value at higher temperatures. In Table 4 we present γ values as a function of altitude at three different latitudes spanning two seasons. These are extrapolations based on our semiempirical theory. Temperature, pressure, and water vapor mixing ratio profiles were calculated using the model described by *Granier and Brasseur* [1992]. The aerosol composition was calculated from work by *Gmitro and Vermeulen* [1964] using these values. As shown, γ is expected to drop from 0.15 to 0.03 as the temperature drops from 207 K to 189 K in the south polar winter stratosphere. The expected drop in γ for the north polar stratosphere is not as dramatic. We must again emphasize the extrapolated nature of these results based on a theory that awaits confirmation by additional studies. Such studies are also needed to determine the aerosol phase and the resulting reaction probability.

Acknowledgments. We thank Geoff Tyndall for many helpful discussions and suggestions during the course of this study. We also thank Richard Shetter for assistance in preparing the N_2O_5; John Lind for help in analyzing the output of our N_2O_5 source; Chuck Wilson for assistance with the tandem DMA measurements; Jack Fox for advice on mechanical details of the apparatus; John Orlando for identification of and help with the formaldehyde measurements; Claire Granier and Guy Brasseur for model calculations of temperature, pressure, and water vapor profiles; and Chris Cantrell, Scott Sewell, and Leon Phillips for many helpful suggestions. This work was supported by a grant from the National Aeronautics and Space Administration. NCAR is supported by the National Science Foundation.

REFERENCES

Austin, J., R. R. Garcia, J. M. Russell III, S. Solomon, and A. F. Tuck, On the atmospheric photochemistry of nitric acid, *J. Geophys. Res., 91*, 5477-5485, 1986.

Baldwin, A. C., and D. M. Golden, Heterogeneous atmospheric reactions: Sulfuric acid aerosols as tropospheric sinks, *Science, 206*, 562-563, 1979.

Berdnikov, V. M., and N. M. Bazhin, Oxidation-reduction potentials of certain inorganic radicals in aqueous solutions, *Russ. J. Phys. Chem., 44*, 395-398, 1970.

Brasseur, G. P., C. Granier, and S. Walters, Future changes in stratospheric ozone and the role of heterogeneous chemistry, *Nature, 348*, 626-628, 1990.

Brown, R. L., Tubular flow reactors with first-order kinetics, *J. Res. Natl. Bur. Stand., 83*, 1-8, 1978.

Cantrell, C. A., J. A. Davidson, R. E. Shetter, B. A. Anderson, and J. G. Calvert, Reactions of NO_3 and N_2O_5 with molecular species of possible atmospheric interest, *J. Phys. Chem., 91*, 6017-6021, 1987.

Considine, D. B., A. R. Douglass, and R. S. Stolarski, Heterogeneous conversion of N_2O_5 to HNO_3 on background stratospheric aerosols: Comparisons of model results with data, *Geophys. Res. Lett., 19*, 397-400, 1992.

Davidovits, P., J. T. Jayne, S. X. Duan, D. R. Worsnop, M. S. Zahniser, and C. E. Kolb, Uptake of gas molecules by liquids: A model, *J. Phys. Chem., 95*, 6337-6340, 1991.

Fahey, D. W., C. S. Eubank, G. Hubler, and F. C. Fehsenfeld, A calibrated source of N_2O_5, *Atmos. Environ., 19*, 1883-1890, 1985.

Frenkel, J., *Kinetic Theory of Liquids*, Dover, Mineola, N.Y. 1955.

Fried, A., J. R. Drummond, B. Henry, and J. Fox, Versatile integrated tunable diode laser system for high precision: Application for ambient measurements of OCS, *Appl. Opt., 30*, 1916-1932, 1991.

Fried, A., B. Henry, and J. R. Drummond, Tunable diode laser ratio measurements of atmospheric constituents by employing dual fitting analysis and jump scanning, *Appl. Opt., 32*, 821-827, 1993.

Fuchs, N. A., *The Mechanics of Aerosols*, Pergamon, New York, 1964.

Fuchs, N. A., and A. G. Sutugin, *Highly Dispersed Aerosols*, Butterworth, Stoneham, Mass., 1970.

Gable, C. M., H. F. Betz, and S. H. Maron, Phase equilibria of the system sulfur trioxide-water, *J. Am. Chem. Soc., 72*, 1445-1448, 1950.

Gmitro, J. I., and T. Vermeulen, Vapor-liquid equilibria for aqueous sulfuric acid, *Am. Inst. Chem. Eng. J., 10*, 740-746, 1964.

Golden, D. M., J. A. Manion, C. M. Reihs, and M. A. Tolbert, Heterogeneous chemistry on global stratospheric particulate: Reaction of $ClONO_2$ and N_2O_5 on sulfuric acid surfaces, in *CHEMRAWN VII, Chemistry of the Atmosphere: The Impact of Global Change*, edited by *J. G. Calvert, Blackwell Scientific Publications Ltd., Oxford University Press*, New York, in press, 1993.

Granier, C., and G. Brasseur, Impact of heterogeneous chemistry on model predictions of ozone changes, *J. Geophys. Res., 97*, 18,015-18,033, 1992.

Grant, W. B., J. Fishman, E. V. Browell, V. G. Brackett, D. Nganga, A. Minga, B. Cros, R. E. Veiga, C. F. Butler, M. A. Fenn, and G. D. Nowicki, Observations of reduced ozone concentrations in the tropical stratosphere after the eruption of Mt. Pinatubo, *Geophys. Res. Lett., 19*, 1109-1112, 1992.

Hanson, D. R., and A. R. Ravishankara, The reaction probabilities of $ClONO_2$ and N_2O_5 on 40 to 75% sulfuric acid solutions, *J. Geophys. Res., 96*, 17,307-17,314, 1991.

Harker, A. B., and D. R. Strauss, Kinetics of the heterogeneous hydrolysis of dinitrogen pentoxide over the temperature range 214-263K, *Fed. Aviat. Admin. Publ. FAA-EE-81-3*, Rockwell Int. Sci. Cent., Thousand Oaks, Calif., 1981.

Hofmann, D. J., and S. Solomon, Ozone destruction through heterogeneous chemistry following the eruption of El Chichon, *J. Geophys. Res., 94*, 5029-5041, 1989.

Jayne, J. T., S. X. Duan, P. Davidovits, D. R. Worsnop, M. S. Zahniser, and C. E. Kolb, Uptake of gas-phase alcohol and organic acid molecules by water surfaces, *J. Phys. Chem., 95*, 6329-6336, 1991.

Johnston, P. V., R. L. McKenzie, J. G. Keys, and W. A. Matthews, Observations of depleted stratospheric NO_2 following the Pinatubo volcanic eruption, *Geophys. Res. Lett., 19*, 211-213, 1992.

Kawa, S. R., D. W. Fahey, L. E. Heidt, W. H. Pollack, S. Solomon, D. E. Anderson, M. Loewenstein, M. H. Proffit, J. J. Margitan, and K. R. Chan, Photochemical partitioning of reactive nitrogen and chlorine reservoirs in the high-latitude stratosphere, *J. Geophys. Res., 97*, 7905-7923, 1992.

Knutson, E. O., and K. T. Whitby, Aerosol classification by electric mobility: Apparatus, theory, and applications, *J. Aerosol Sci., 6*, 443-451, 1975.

Langhaar, H. L., Steady flow in the transition region of a straight tube, *J. Appl. Mech., 9*, A55-A58, 1942.

Lee, K. W., H. Chen, and J. A. Gieseke, Log-normally preserving size distribution for Brownian coagulation in the free-molecule regime, *Aerosol Sci. Technol., 3*, 53-62, 1984.

Liu, B. Y. H., and D. Y. H. Pui, Equilibrium bipolar charge distribution of aerosols, *J. Colloid Interface Sci., 49*, 305-312, 1974.

McMurry, P. H., and D. J. Rader, Aerosol wall losses in electrically charged chambers, *Aerosol. Sci. Technol., 4*, 249-268, 1985.

Mozurkewich, M., Aerosol growth and the condensation coefficient for water: A review, *Aerosol Sci. Technol., 5*, 223-236, 1986.

Mozurkewich, M., and J. G. Calvert, Reaction probability of N_2O_5 on aqueous aerosols, *J. Geophys. Res., 93*, 15,889-15,896, 1988.

Murphy, D. M., and D. W. Fahey, Mathematical treatment of the wall loss of a trace species in denuder and catalytic converter tubes, *Anal. Chem., 59*, 2753-2759, 1987.

Patrick, R., and D. M. Golden, Third-order rate constants of atmospheric importance, *Int. J. Chem. Kinet., 15*, 1189-1227, 1983.

Perry, R. H., and C. H. Chilton, *Chemical Engineers' Handbook*, 5th ed., McGraw-Hill, New York, 1978.

Pitari, G., G. Visconti, and V. Rizi, Sensitivity of stratospheric ozone to heterogeneous chemistry on sulfate aerosols, *Geophys. Res. Lett., 18*, 833-836, 1991.

Prather, M., Catastrophic loss of stratospheric ozone in dense volcanic clouds, *J. Geophys. Res., 97*, 10187-10191, 1992.

Rader, D. J., and P. H. McMurry, Application of the tandem differential mobility analyzer to studies of droplet growth or evaporation, *J. Aerosol Sci., 17*, 771-787, 1986.

Reid, R. C. and T. K. Sherwood, *The Properties of Gases and Liquids*, 2nd ed., McGraw-Hill, New York, 1966.

Rodriguez, J. M., M. K. W. Ko, and N. D. Sze, Role of heterogeneous conversion of N_2O_5 on sulphate aerosols in global ozone losses, *Nature, 352*, 134-137, 1991.

Roscoe, H. K., B. J. Kerridge, L. J. Gray, R. J. Wells, and J. A. Pyle, Simultaneous measurements of stratospheric NO and NO_2 and their comparison with model predictions, *J. Geophys. Res., 91*, 5405-5419, 1986.

Sabinina, L., and L. Terpugow, Die Oberflachenspannung des Systems Schwefelsaure-Wasser, *Z. Phys. Chem., Abt. A173*, 237-241, 1935.

Schwartz, S. E., Mass transport considerations pertinent to aqueous-phase reactions of gases in liquid-water clouds, in *Chemistry of Multiphase Atmospheric Systems*, edited by W. Jaeschke, Springer-Verlag, New York, 415-471, 1986.

Schwartz, S. E., and J. E. Freiberg, Mass-transport limitation to the rate of reaction of gases in liquid droplets: Application to oxidation of SO_2 in aqueous solutions, *Atmos. Environ., 15*, 1129-1145, 1981.

Solomon, S., The mystery of the Antarctic ozone "hole," *Rev. Geophys., 26*, 131-148, 1988.

Turco, R. P., R. C. Whitten, and O. B. Toon, Stratospheric aerosols: Observation and theory, *Rev. Geophys. Space Phys., 20*, 233-279, 1982.

Turco, R. P., O. B. Toon, and P. Hamill, Heterogeneous physicochemistry of the polar ozone hole, *J. Geophys. Res., 94*, 16,493-16,510, 1989.

Van Doren, J. M., L. R. Watson, P. Davidovits, D. R. Worsnop, M. S. Zahniser, and C. E. Kolb, Uptake of N_2O_5 and HNO_3 by aqueous sulfuric acid droplets, *J. Phys. Chem., 95*, 1684-1689, 1991.

Walker, K. L., G. M. Homsy, and F. T. Geyling, Thermophoretic deposition of small particles in laminar tube flow, *J. Colloid Interface Sci., 69*, 138-147, 1979.

Washburn, E. W. (Ed.), *International Critical Tables of Numerical Data, Physics, Chemistry and Technology*, McGraw-Hill, New York, 1928.

Yao, L. S., Is fully developed and non-isothermal flow possible in a vertical pipe?, *Int. J. Heat Mass Transfer, 30*, 707-716, 1987a.

Yao, L. S., Linear stability analysis for opposing mixed convection in a vertical pipe, *Int. J. Heat Mass Trans., 30*, 810-811, 1987b.

Zhang, Z., and B. Y. H. Liu, Performance of TSI 3760 condensation nucleus counter at reduced pressures and flow rates, *Aerosol Sci. Technol., 15*, 228-238, 1991.

J. G. Calvert, A. Fried, and B. Henry, National Center for Atmospheric Research, P. O. Box 3000, Boulder, CO 80307.

M. Mozurkewich, Department of Chemistry and Centre for Atmospheric Chemistry, York University, 4700 Keele Street, North York, Ontario M3J IP3, Canada.

(Received March 10, 1993; revised June 20, 1993; accepted July 9, 1993.)